parameters such as tryptic cleavage specificity, precursor ion mass accuracy, and fragment ion mass accuracy were set using built-in functions of the software. After protein identification, the data were further processed using the ProGroup algorithm within ProteinPilot to determine the minimal justifiable set of identified proteins. Relative abundances of proteins were calculated based on individual peptide ratios. Peptides shared among identified proteins were not included for relative quantitation. Isoform-specific relative quantitation was carried out by selecting peptides distinct to each form.

For protein identification, our criterion was the 95% confidence score cutoff (≥1.3 unused ProtScore). The *p*-value correlation analysis was calculated using the ProteinPilot software, and standard deviations were analyzed using the Statcel2 software (OMS, Saitama, Japan). In addition, we performed background noise reduction and bias correction in ProteinPilot, and then calculated the protein false discovery rate using the built-in PSPEP algorithm [22].

2.3. *Functional analysis*

For the downstream bioinformatic analysis, the differentially expressed fish protein sequences detected by proteome analysis were first searched against the human protein database (15,381 entries, NCBI nr, accessed April 14 2009) using the NCBI BLASTP program set to find homologous sequences. For the functional analysis, we used Ingenuity Pathways Analysis [(IPA), Ingenuity Systems, www.ingenuity.com] equipped with the Ingenuity Pathways Knowledge Base. By IPA, the assigned proteins were classified according to subcellular localization, molecular functions, and biological functions, based on information contained in the Ingenuity Pathways Knowledge Base.

2.4. *Construction of GH1-Tg amago salmon*

Production of GH1 transgenic amago salmon was performed as previously described [23]. Both homozygous (homo) and heterozygous (hetero) amago salmons were derived from a single *O. masou* founder that expressed the gene construct (OnMTGH1). The construct itself comprised of the MT-B promoter from sockeye salmon (*Oncorhynchus nerka*) fused to the coding region of their type 1 GH gene. Non-Tg and GH1-Tg (both homo and hetero) were siblings. After ice anesthesia, their body weight was measured, and pituitary and blood from the caudal vasculature were collected. Blood was kept on ice followed by centrifugation at 750 g for 15 min to obtain plasma samples, which were stored at −80 °C until assayed for measurement of GH1, Insulin-like growth factor I (IGF-I) and lipid metabolites. Meanwhile, the collected pituitaries were used for transcriptome analysis as described below.

2.5. *Measurement of GH1, IGF-I, and lipid metabolites in plasma*

Plasma samples were extracted according to the method of Shimizu et al. (2000) [24]. Levels of GH1 and IGF-I in plasma were measured by homologous radioimmunoassays (RIAs) according to the methods of Swanson (1994) [25] and Moriyama et al. (1994) [26] with slight modifications. Radioactivity of anti-GH1 or anti-IGF-I antibody-bound hormone complexes, which were precipitated with 100 ml of 0.25% PANSORBIN Cells (Calbiochem, Darmstadt, Germany) suspended in RIA buffer, was counted using a Packard COBRA gamma counter (GMI, Ramsey, MN, USA). The lowest detectable levels of GH1 and IGF-I were 0.75 ng/ml and 1.78 ng/ml, respectively. Intra-assay coefficient of variation was less than 5%. Cholesterol and triglyceride concentrations in the serum were determined using a Fuji DRI-CHAM Auto-5 automated analyzer system (Fuji Film, Tokyo, Japan).

2.6. *Quantitative real-time PCR*

Quantitative real-time PCR was performed according to the manufacturer's instructions. Total RNA was extracted from pituitary of GH1-Tg and non-Tg amago salmon using an RNeasy Micro kit (Qiagen, Duesseldorf, Germany). cDNA, from total RNA (1 μg), was synthesized using a Prime Script RT reagent Kit (TAKARA Bio, Shiga, Japan) with oligo dT_{20} random 6-mer primers . Quantitative real-time PCR (qRT-PCR) was performed on a Mx3000P Real-Time QPCR System (Agilent Technologies, Santa Clara, CA, USA) using SYBR Premix Ex Taq II (TAKARA Bio). The mRNA levels of GH1 genes were determined using the $2^{-\Delta\Delta C}$T comparative method. The 18S rRNA was used as the reference genes. Primer sequences are listed in Table 1.

2.7. *Transcriptome analysis using amago salmon-specific subtractive microarray*

To produce an amago salmon-specific subtractive microarray, we constructed subtractive cDNA libraries from 1 μg total RNA from GH1-Tg and non-Tg pituitary, using PCR-Select cDNA Subtraction Kits (Clontech, Mountain View, CA, USA) combined with the SMART PCR cDNA Synthesis kit (Clontech). Differentially expressed cDNA clones were randomly picked and sequenced using BigDye Terminator v3.1/1.1 Cycle Sequencing kits (Applied Biosystems, Foster City, CA, USA), and then identified using the NCBI BLASTN program. cDNA from 1915 independent clones was amplified by PCR, using primers flanking the cloning site (unpublished information). These DNAs, as well as external positive and negative control DNAs, were spotted onto glass microarray slides in triplicate (5760 spots). Aminoallyl-labeled antisense RNA microarray probes were synthesized from GH1-Tg or non-Tg total RNAs (1 μg) using the MessageAmpII aRNA Amplification Kit (Ambion, Foster City, CA, USA). These RNA probes (8 μg) were

Table 1 – Primer list for RT-PCR analysis.

(1) GH1 common primers
Forward: 5′-CTGATGAACGCAGACAGC-3′
Reverse: 5′-CCAGGATTCAATCAGACGG-3′
(2) GH1 transgene-specific primers (transgene is from sockeye salmon)
Forward: 5′-AATTCTCCCAGCGTCGTTAG-3′
Reverse: 5′-CCAGGATTCAATCAGACGG-3′
(3) Amago-specific primers
Forward: 5′-GATATTCCTGCTGGACTTC-3′
Reverse: 5′-GATGGTTTTACTTGCAATGATTGTG-3′
(3) 18S rRNA (control) primers
Forward: 5′-GGTGGAGCGATTTGTCTGG-3′
Reverse: 5′-CTCAATCTCGTGTGGCTGAAG-3′

coupled with Cy5 or Cy3 dye. Microarray analysis, which included dye-swap experiments to compensate for dye-specific labeling effect, was repeated by using five independently generated salmon probes. Detailed protocols for hybridization, signal scanning and microarray processing have been described in a previous report [23,27].

Background signals were subtracted from the raw data, and the data were then subjected to Lowess normalization (locally weighted scatter plot smoothing) between the Cy5 and Cy3 channels. Signal intensities under 1000 were eliminated. The average signal intensities of Cy5 and Cy3 were obtained, and the dye-swap log ratios (GH1-Tg/non-Tg) were calculated as the logarithm of the ratios of the Cy5 and Cy3 intensities. These transformed dye-swap log ratios were analyzed using an unpaired Student's t-test (fold change >1.5, $p<0.05$ corrected by Benjamini–Hochberg FDR) using the Avadis 4.3 software (Strand Inc., Bangalore, India).

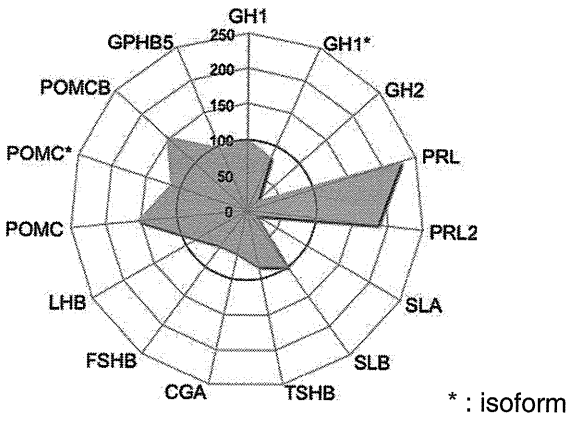

Fig. 2 – Expression levels of pituitary hormones affected by excess GH1 treatment. The green chart indicates the levels of pituitary hormones expressed at different levels in the excess GH1-treated vs. non-treated pituitary. Red circle indicates expression levels of pituitary hormones in non-treated pituitary. Asterisks indicate isoforms of identical pituitary hormone.

3. Results and discussion

3.1. *Protein profile in salmon pituitary treated with GH1*

In order to identify pituitary proteins that specifically increase or decrease in response to excess GH1, we performed comprehensive and quantitative proteome analysis using iTRAQ

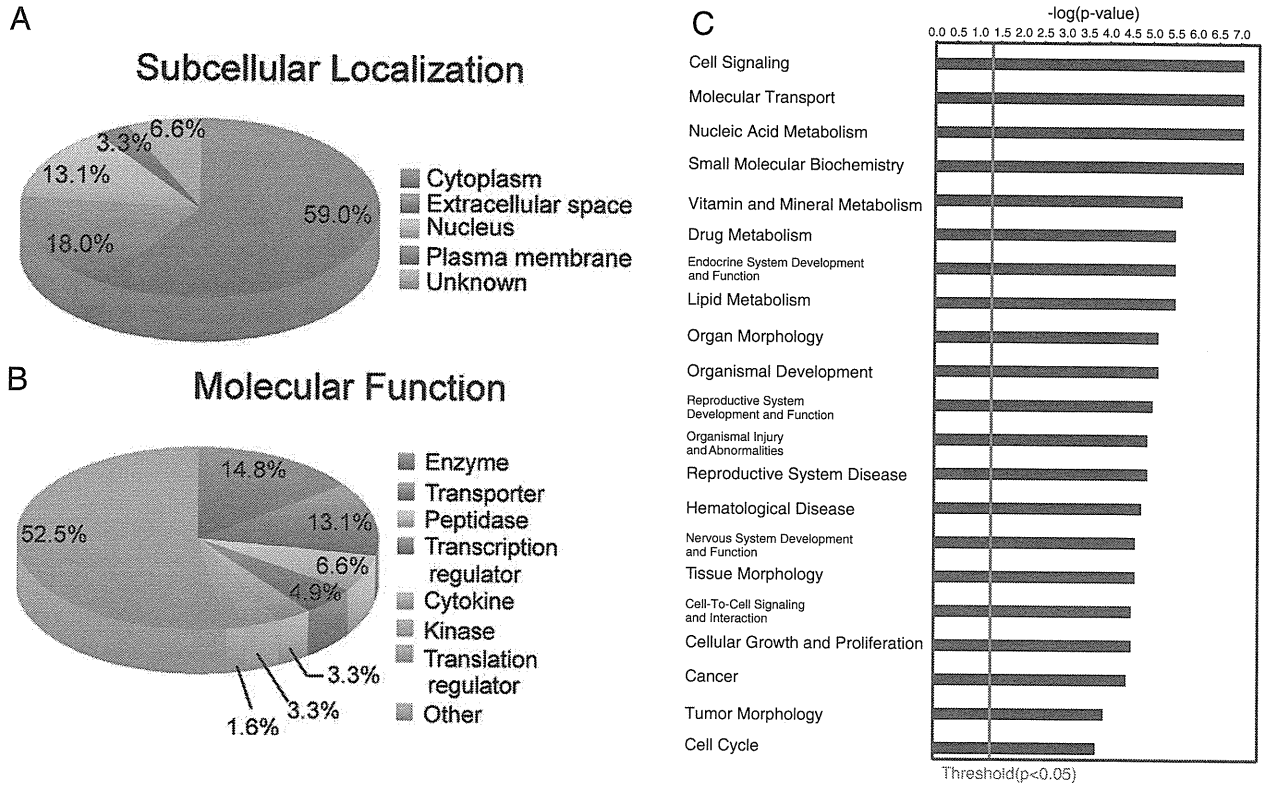

Fig. 1 – Functional classification of pituitary proteins differentially expressed in response to excess GH1 treatment. (A) Subcellular localization of proteins differentially expressed in the excess GH1-treated pituitary compared to non-treated pituitary. Sixty-one proteins with human homologs were classified into each annotation category by the Ingenuity Pathways Knowledge Base. (B) Molecular functions of the differentially expressed proteins described in Fig. 1A. (C) Biological functions associated with 61 homologous human proteins, obtained from the Ingenuity Pathways Knowledge Base. Fisher's exact test was used to calculate a p-value (threshold $p<0.05$) for each biological function.

Table 2A

Name	Accession	iTRAQ peptides	Unused	%Cov	Entrez Gene Name(Human homolog)	Symbol (Human)	Entrez GENE ID (Human)
Prolactin	gi|185132553	115	29.9	79.04999852	Prolactin	PRL	5617
Similar to Granzyme-like protein 1 precursor (GLP-1)	gi|189535255	1	1.84	11.11000031	Granzyme B (granzyme 2, cytotoxic T-lymphocyte-associated serine esterase 1)	GZMB	3002
Prolactin II	gi|41019311	8	1.53	36.10999882			
26S proteasome non-ATPase regulatory subunit 4	gi|209736020	1	2.02	11.14000008	Proteasome (prosome, macropain) 26S subunit, non-ATPase, 4	PSMD4	5710
Heterogeneous nuclear ribonucleoprotein A1	gi|223647288	9	31.63	68.22999716	Heterogeneous nuclear ribonucleoprotein A1	HNRNPA1	3178
Unnamed protein product	gi|47222767	1	2.09	9.316000342	Rho guanine nucleotide exchange factor (GEF) 19	ARHGEF19	128272
Melanin-concentrating hormone precursor	gi|213457	17	5.52	53.7899971	Pro-melanin-concentrating hormone	PMCH	5367
Proopiomelanocortine A	gi|185132704	20	8.51	32.01999962	Proopiomelanocortin	POMC	5443
Proopiomelanocortin	gi|530904	7	2	46.90000117	Proopiomelanocortin	POMC	5443
Isotocin / neurophysin 1 precursor	gi|418825	12	5.7	13.2100001	Arginine vasopressin	AVP	551
Unnamed protein product	gi|47219657	1	2.02	12.88000047	Ubiquitin specific peptidase 7 (herpes virus-associated)	USP7	7874
Clathrin light chain A	gi|209731460	1	2.06	33.32999945	Clathrin, light chain A	CLTA	1211
Unnamed protein product	gi|47230642	11	11.91	28.74000072	Secretogranin III	SCG3	29106
PHD finger protein 17	gi|41054211	1	1.71	7.117000222	PHD finger protein 17	PHF17	79960
60 kDa heat shock protein, mitochondrial precursor	gi|209153200	2	6.41	20.20999938	Heat shock 60kDa protein 1 (chaperonin)	HSPD1	3329
S100-B [Salmo salar]	gi|226443324	1	4	38.94999921	S100 calcium binding protein B	S100B	6285
ATP synthase H+ transporting mitochondrial F1 complex beta	gi|198285477	89	45.41	75.34999847	ATP synthase, H+ transporting, mitochondrial F1 complex, beta polypeptide	ATP5B	506
Myosin light chain 2	gi|7678750	1	1.81	11.76000014	Myosin light chain, phosphorylatable, fast skeletal muscle	MYLPF	29895
Actin-related protein 2/3 complex subunit 5	gi|223647102	1	2.02	20.0000003	Actin related protein 2/3 complex, subunit 5, 16kDa	ARPC5	10092
Tubulin beta-3 chain	gi|213514092	3	2.1	47.87999988	Tubulin, beta 3	TUBB3	10381
Mitochondrial import receptor subunit TOM22 homolog	gi|225707812	1	2	9.701000154	Translocase of outer mitochondrial membrane 22 homolog (yeast)	TOMM22	56993
NADP-dependent malic enzyme, mitochondrial precursor	gi|223647696	1	2	3.582999855	Malic enzyme 3, NADP(+)-dependent, mitochondrial	ME3	10873
Tubulin alpha chain	gi|267071	2	2	70.95000148	Tubulin, alpha 1c	TUBA1C	84790
Unnamed protein product	gi|47212864	2	1.85	6.173000112	Myosin XVIIIA	MYO18A	399687
Hypothetical protein	gi|164518348	1	1.52	3.458999842	Orofacial cleft 1 candidate 1	OFCC1	266553
Proteasome subunit beta type 2	gi|225705784	1	2.05	23.49999994	Proteasome (prosome, macropain) subunit, beta type, 2	PSMB2	5690
Creatine kinase B-type	gi|213513714	34	24.21	71.39000297	Creatine kinase, brain	CKB	1152
Vacuolar ATP synthase catalytic subunit A	gi|224587380	1	2	47.27999866	ATPase, H+ transporting, lysosomal 70kDa, V1 subunit A	ATP6V1A	523

Sept2 protein	gi|94574481	1	2.01	10.39000005	Septin 2	SEPT2	4735
Similar to restin	gi|189524793	1	1.7	10.44000015	CAP-GLY domain containing linker protein 1	CLIP1	6249
Neuromodulin	gi|213513358	1	3.17	19.28000003	Growth associated protein 43	GAP43	2596
DnaJ homolog subfamily C member 3	gi|213510886	1	1.4	12.20000014	DnaJ (Hsp40) homolog, subfamily C, member 3	DNAJC3	5611
Unnamed protein product	gi|47228465	1	4.1	29.31999862	Heterogeneous nuclear ribonucleoprotein D (AU-rich element RNA binding protein 1, 37kDa)	HNRNPD	3184
Hyperosmotic glycine rich protein-like	gi|198285593	10	12.58	75.62999725	Cold inducible RNA binding protein	CIRBP	1153
Unnamed protein product	gi|47218197	1	2.21	9.765999764	Calcium/calmodulin-dependent protein kinase II gamma	CAMK2G	818
Small nuclear ribonucleoprotein-associated protein B	gi|213512296	1	2.01	27.00000107	Small nuclear ribonucleoprotein polypeptide N	SNRPN	6638
Glyceraldehyde-3-phosphate dehydrogenase	gi|225715600	1	4.01	32.73000121	Glyceraldehyde-3-phosphate dehydrogenase	GAPDH (includes EG:2597)	2597
4-aminobutyrate aminotransferase, mitochondrial precursor	gi|209154560	1	1.58	15.19999951	4-aminobutyrate aminotransferase	ABAT	18
Aldolase a, fructose-bisphosphate 1	gi|213511774	1	3.74	43.79999936	Aldolase C, fructose-bisphosphate	ALDOC	230
Unnamed protein product	gi|47216776	1	2	14.49999958	Vacuolar protein sorting 29 homolog (S. cerevisiae)	VPS29	51699
Novel protein similar to human general control of amino-acid synthesis 1-like 1	gi|33284844	1	1.45	4.444999993	GCN1 general control of amino-acid synthesis 1-like 1 (yeast)	GCN1L1	10985
60S ribosomal protein L24	gi|209731598	1	2.91	15.28999954	Ribosomal protein L24	RPL24	6152
Triosephosphate isomerase	gi|209734404	46	12.25	53.22999954	Triosephosphate isomerase 1	TPI1	7167
Proprotein convertase subtilisin/kexin type 1	gi|212549686	1	2.95	9.66899991	Proprotein convertase subtilisin/kexin type 1	PCSK1	5122
Hemoglobin subunit beta	gi|209735786	1	2.18	95.27000189	Hemoglobin, beta	HBB (includes EG:3043)	3043
Prothymosin alpha	gi|221221610	4	10	44.13999915	Prothymosin, alpha	PTMA	5757
Unnamed protein product	gi|47222619	1	2.58	9.464000165	Apoptosis-inducing factor, mitochondrion-associated, 1	AIFM1	9131
Alpha-globin 4	gi|162949430	23	15.96	62.94000149	Hemoglobin, alpha 2	HBA2	3040
Hemoglobin subunit beta-1	gi|225703790	48	24.03	89.80000019	Hemoglobin, gamma A	HBG1	3047
Calreticulin	gi|185134556	8	36.38	60.61999798	Calreticulin	CALR	811
Unnamed protein product	gi|47214161	1	1.73	20.6400007	Enoyl CoA hydratase domain containing 2	ECHDC2	55268
SMEK homolog 2	gi|223647852	1	1.74	6.795000285	SMEK homolog 2, suppressor of mek1 (Dictyostelium)	SMEK2	57223
Unnamed protein product	gi|47203923	2	2	6.168999895	Actin filament associated protein 1-like 2	AFAP1L2	84632
Gonadotrophin alpha 1 subunit	gi|546258	18	8.22	63.02999854	Glycoprotein hormones, alpha polypeptide	CGA	1081
Follicle stimulating hormone beta subunit	gi|45685133	5	6.8	29.19999957	Follicle stimulating hormone, beta polypeptide	FSHB	2488
Hypothetical protein LOC335859	gi|189526442	1	2.03	4.540000111	Fatty acid synthase	FASN	2194
Dynactin subunit 2	gi|209155422	5	5.97	23.2099995	Dynactin 2 (p50)	DCTN2	10540
Melanin concentrating hormone 2 (MCH2) precursor	gi|213455	16	5.82	41.67000055	Pro-melanin-concentrating hormone	PMCH	5367
60S acidic ribosomal protein P2	gi|225703274	1	3.85	57.88999796	Ribosomal protein, large, P2	RPLP2	6181
Rho GDP-dissociation inhibitor 1	gi|209154488	5	5.18	36.75999939	Rho GDP dissociation inhibitor (GDI) alpha	ARHGDIA	396
Hypothetical protein LOC569455	gi|224496028	1	1.42	4.828000069	Importin 5	IPO5	3843
Growth hormone 2	gi|159032827	40	23.93	87.13999987	Growth hormone 1	GH1	2688
Somatolactin (alpha)	gi|134726	74	27.38	64.38000202			

Table 2B

Name	Fold Change	StDev	PVal	EF	Lower CI	Upper CI	Location	Type(s)
	GH1-treated / Non-treated	GH1-treated / Non-treated	GH1-treated / Non-treated	GH1-treated / Non-treated	GH1-treated / Non-treated	GH1-treated / Non-treated		
Prolactin	2.290868044	0.011725673	0.002106669	1.270573974	1.803017974	5.915616989	Extracellular space	Cytokine
Similar to Granzyme-like protein 1 precursor (GLP-1)	1.870682001		0.349433392	2.089296103	0.895364821	3.944572926	Cytoplasm	Peptidase
Prolactin II	1.853531957	0.02704107	0.42510739	1.202263951	1.541700006	2.355048895		
26S proteasome non-ATPase regulatory subunit 4	1.803017974		0.367049694	2.089296103	0.862978518	3.80189395	Cytoplasm	Other
Heterogeneous nuclear ribonucleoprotein A1	1.721868992	0.089899039	0.497172803	1.614359021	1.066596031	6.08134985	Nucleus	Other
Unnamed protein product	1.599557996		0.435547709	2.089296103	0.765596628	3.372873068	unknown	Other
Melanin-concentrating hormone precursor	1.584892988	0.066547362	0.428161502	1.342764974	1.180320978	2.582259893	Extracellular space	Other
Proopiomelanocortine A	1.55596602	0.016729234	0.672467113	1.180320978	1.318256974	2.089296103	Extracellular space	Other
Proopiomelanocortin	1.541700006	0.063988531	0.562245309	1.472311974	1.047129035	2.703958035	Extracellular space	Other
Isotocin / neurophysin 1 precursor	1.527565956	0.039493514	0.617341816	1.355188966	1.127197981	3.66437602	Extracellular space	Other
Unnamed protein product	1.499685049		0.482902408	2.108628035	0.711213529	3.133285999	Nucleus	Peptidase
Clathrin light chain A	1.445440054		0.513746679	2.108628035	0.685488224	3.019952059	Plasma membrane	Other
Unnamed protein product	1.432188034	0.069806954	0.367831409	1.432188034	1	2.630268097	Extracellular space	Other
PHD finger protein 17	1.380383968		0.549392521	2.089296103	0.660693526	2.91071701	Nucleus	Other
60 kDa heat shock protein, mitochondrial precursor	1.367728949	0.014446496	0.394513786	2.089296103	0.654636085	2.85758996	Cytoplasm	Enzyme
S100-B [Salmo salar]	1.367728949		0.558983624	2.089296103	0.654636085	2.884032011	Cytoplasm	Other
ATP synthase H+ transporting mitochondrial F1 complex beta	1.355188966	0.024410988	0.04585408	1.14815402	1.180320978	1.584892988	Cytoplasm	Transporter
Myosin light chain 2	1.355188966		0.56853348	2.089296103	0.648634374	2.83139205	Cytoplasm	Other
Actin-related protein 2/3 complex subunit 5	1.342764974		0.575936973	2.089296103	0.642687678	2.83139205	Cytoplasm	Other
Tubulin beta-3 chain	1.330453992	0.037739066	0.53627342	1.419057012	0.937561989	1.887990952	Cytoplasm	Other
Mitochondrial import receptor subunit TOM22 homolog	1.330453992		0.58843261	2.089296103	0.636795521	2.779712915	Cytoplasm	Transporter
NADP-dependent malic enzyme, mitochondrial precursor	1.318256974		0.601977408	2.108628035	0.625172675	2.754229069	Cytoplasm	Enzyme
Tubulin alpha chain	1.318256974	0.023815861	0.575083613	2.089296103	0.630957425	2.779712915	Cytoplasm	Other
Unnamed protein product	1.318256974	0.051703542	0.535494089	2.089296103	0.630957425	2.779712915	Cytoplasm	Other
Hypothetical protein	1.30617094		0.605844915	2.089296103	0.625172675	2.728977919	unknown	Other
Proteasome subunit beta type 2	1.29419601		0.62100333	2.108628035	0.613762021	2.703958035	Cytoplasm	Peptidase
Creatine kinase B-type	1.28233099	0.040311887	0.324288607	1.235947013	1.037528038	1.737800956	Cytoplasm	Kinase
Vacuolar ATP synthase catalytic subunit A	1.28233099		0.625988781	2.089296103	0.613762021	2.703958035	Cytoplasm	Transporter
Sept2 protein	1.28233099		0.626250029	2.089296103	0.613762021	2.703958035	Cytoplasm	Enzyme

Similar to restin	1.270573974		0.644315183	2.108628035	0.602559626	2.654606104	Cytoplasm	Other
Neuromodulin	1.258924961		0.650084972	2.089296103	0.602559626	2.630268097	Plasma membrane	Other
DnaJ homolog subfamily C member 3	0.794328213		0.667952716	2.089296103	0.376703799	1.659587026	Cytoplasm	Other
Unnamed protein product	0.794328213		0.674318373	2.089296103	0.380189389	1.659587026	Nucleus	Transcription regulator
Hyperosmotic glycine rich protein-like	0.787045777	0.041524451	0.524631321	1.247382998	0.591561615	0.981747925	Nucleus	Other
Unnamed protein product	0.787045777		0.657890975	2.089296103	0.373250186	1.644371986	Cytoplasm	Kinase
Small nuclear ribonucleoprotein-associated protein B	0.779830098		0.650910974	2.089296103	0.373250186	1.629295945	Nucleus	Other
Glyceraldehyde-3-phosphate dehydrogenase	0.765596628		0.629889786	2.089296103	0.366437614	1.599557996	Cytoplasm	Enzyme
4-aminobutyrate aminotransferase, mitochondrial precursor	0.758577585		0.622181296	2.108628035	0.363078088	1.599557996	Cytoplasm	Enzyme
Aldolase a, fructose-bisphosphate 1	0.758577585		0.61985302	2.108628035	0.363078088	1.599557996	Cytoplasm	Enzyme
Unnamed protein product	0.758577585		0.620348215	2.108628035	0.363078088	1.599557996	Cytoplasm	Transporter
Novel protein similar to human general control of amino-acid synthesis 1-like 1	0.751622915		0.608968377	2.089296103	0.359749287	1.570363045	Cytoplasm	Translation regulator
60S ribosomal protein L24	0.731139123		0.58094883	2.108628035	0.349945188	1.541700006	Cytoplasm	Other
Triosephosphate isomerase	0.731139123	0.020682539	0.375185192	1.16949904	0.515228629	0.855066717	Cytoplasm	Enzyme
Proprotein convertase subtilisin/kexin type 1	0.717794299		0.565635085	2.108628035	0.343558013	1.51356101	Extracellular space	Peptidase
Hemoglobin subunit beta	0.711213529		0.548802316	2.089296103	0.337287307	1.485936046	Cytoplasm	Transporter
Prothymosin alpha	0.691830993	0.041728616	0.526520073	1.419057012	0.373250186	0.981747925	Nucleus	Transcription regulator
Unnamed protein product	0.685488224		0.515590072	2.089296103	0.325087309	1.432188034	Cytoplasm	Enzyme
Alpha-globin 4	0.679203629	0.130065185	0.892440081	1.472311974	0.405508488	1	Cytoplasm	Transporter
Hemoglobin subunit beta-1	0.679203629	0.029096079	0.370831192	1.224616051	0.165958703	0.831763685	Cytoplasm	Transporter
Calreticulin	0.660693526	0.087643152	0.574053884	1.584892988	0.187068194	1.047129035	Cytoplasm	Transcription regulator
Unnamed protein product	0.648634374		0.471870601	2.089296103	0.307609707	1.355188966	unknown	Other
SMEK homolog 2	0.625172675		0.450730801	2.108628035	0.299226493	1.318256974	unknown	Other
Unnamed protein product	0.625172675	0.003137056	0.454783201	2.108628035	0.299226493	1.318256974	Cytoplasm	Other
Gonadotrophin alpha 1 subunit	0.625172675	0.035022072	0.778641701	1.29419601	0.291071713	0.809095919	Extracellular space	Other
Follicle stimulating hormone beta subunit	0.619441092	0.045384203	0.358060092	1.380383968	0.383707315	0.855066717	Extracellular space	Other
Hypothetical protein LOC335859	0.586138189		0.409159511	2.108628035	0.280543387	1.235947013	Cytoplasm	Enzyme
Dynactin subunit 2	0.529663384	0.019913448	0.269459903	1.570363045	0.017701089	0.831763685	Cytoplasm	Other
Melanin concentrating hormone 2 (MCH2) precursor	0.510505021	0.189016216	0.694045424	1.940886021	0.27289781	0.990831971	Extracellular space	Other
60S acidic ribosomal protein P2	0.428548515		0.27934891	2.108628035	0.205116197	0.90364939	Cytoplasm	Other
Rho GDP-dissociation inhibitor 1	0.398107201	0.127483736	0.273517191	2.290868044	0.021086279	0.912010789	Cytoplasm	Other
Hypothetical protein LOC569455	0.325087309		0.216371298	2.108628035	0.154170096	0.685488224	Nucleus	Transporter
Growth hormone 2	0.207014099	0.076665109	0.229496703	2.398833036	0.098174803	0.496592313	Extracellular space	Cytokine
Somatolactin (alpha)	0.1458814	0.06390252	6.09E-05	3.311311007	0.046989411	0.48305881		

reagents and MS/MS in the amago salmon pituitary, treated (or not) with excess GH1.

In the iTRAQ-MS/MS analysis, we identified 1178 unique proteins (confidence > 95%) from 26,800 spectra; 569 unique proteins at the 5% FDR threshold level. Additionally, by the statistical analysis performed using the ProteinPilot 3.0 software, we defined 63 unique proteins that exhibited differential expression (≥1.25-fold change) in pituitaries cultured with excess GH1.

In order to understand the function of the differentially expressed proteins, we used the IPA software to classify these proteins according to their subcellular localizations, molecular functions, and biological functions. In this analysis, because the fish protein database is not rich in functional information compared to databases for human and mouse, we used BLAST to cross-reference the differentially expressed proteins with their counterparts in the human non-redundant protein database. Among the 63 unique proteins, 61 were identified as having human homologs.

First, these 61 differentially expressed proteins were classified into five discrete subcellular localization categories (cytoplasm, nucleus, plasma membrane, extracellular space, and other). About half of the differentially expressed proteins (59.0%) are localized to the cytoplasm (Fig. 1A).

Second, we classified the 61 proteins into the following eight categories based on their molecular function: enzyme, transporter, peptidase, transcription regulator, cytokine, kinase, translation regulator, and other. Among the 61 proteins, 52.5% of the differentially expressed proteins were classified into multiple categories; 39.4% were classified in single categories as either enzyme (14.8%), transporter (13.1%), peptidase (6.6%) or transcriptional regulation (4.9%) (Fig. 1B).

Third, we classified the proteins based on their biological function ontology. This analysis revealed that many of the proteins that are differentially expressed in response to excess GH1 treatment are molecules related to endocrine systems, cell growth and proliferation, and metabolism (Fig. 1C).

3.1.1. *Endocrine systems*

Fig. 2 indicates the expression levels of peptide hormones in the excess GH1-treated pituitary. In this study, although the expression of endogenous GH1 did not change in response to excess GH1 treatment, levels of the paralogous GH2 decreased; those data suggest that GH2 expression in the amago salmon pituitary is suppressed by excess GH1 treatment.

Another pituitary hormone, somatolactin (SL), which belongs to the GH/PRL family, has been identified only in fishes. SL has two isoforms (SLA and SLB), which are expressed in different sites within the pituitary [28]. Although SL plays important roles in growth, reproduction and metabolism, the functional difference (if any) between SLA and SLB remains unclear. In the proteome analysis, the expression level of SLA, but not SLB, decreased markedly in the GH1-treated pituitary; those data suggest that the two isoforms of SL might be differently regulated by excess GH1 treatment, just as GH1 and GH2 are. However, it is still not clear how differences in expression levels among isoforms of GH and SL affect physiological functions in salmon.

In contrast, two isoforms (PRL1 and PRL2) of PRL, a peptide hormone belonging to GH family, were increased in the excess GH1-treated pituitary (Fig. 2). PRL stimulates increases in food intake and body weight [4]. PRL2 is expressed only in fish, and its function has been postulated to be similar to that of PRL [29]. Up-regulation of both PRL1 and PRL2 in the pituitary in response to excess GH1 treatment might be involved in enhancement of food intake and increase of body weight.

Proteome analysis indicated that glycoprotein hormone FSH, consisting of an α-subunit (CGA) and β-subunit (FSHB), was also decreased in the excess GH1-treated pituitary (Fig. 2). FSH is a major regulator of gonadal development, and is required for oogenesis in females and spermatogenesis in males. Further, inhibition of the FSH receptor induces abnormalities in ovogenesis and spermatogenesis in salmon [6]. Thus, the down-regulation of FSH in the pituitary by excess GH1 treatment might induce attenuation of gonadal development and abnormal fertility. Furthermore, CGA is a subunit of another pituitary glycoprotein hormone, TSH and LH, whose β-subunits are TSHB and LHB, respectively [1,2]. Therefore, down-regulation of CGA by excess GH1 treatment might affect formation and functions of TSH and LH even though levels of LHB and TSHB do not change.

The expression levels of proteins related to hormone production of pituitary also changed in response to excess GH1 treatment (Table 2). PHD finger protein 17 (PHF17) is an E3 ubiquitin ligase that targets β-catenin for proteasomal degradation [30]. β-Catenin is a major component of cell–cell adherence junctions; in the pituitary, it plays a role in cellular organization and cell–cell signaling, which are important for production and secretion of pituitary hormone [31]. Therefore, in the excess GH1-treated pituitary, up-regulation of PHF17 might influence production and secretion of pituitary hormone via the disruption of the pituitary cell network, mediated by downregulation of β-catenin.

Calcium/calmodulin-dependent protein kinase II γ (CAMK2G) is one component of calcium/calmodulin-dependent kinase II (Ca/CAMK II), and plays a key role as a calcium signaling mediator in various tissues, including the pituitary. In the pituitary, Ca/CAMK II increases the mRNA expression level of some pituitary hormones [32,33]. Thus, down-regulation of CAMK2G would presumably affect the expression levels of these hormones (Table 2). Proprotein convertase subtilisin/kexin type 1 (PCSK1), which is expressed in brain and endocrine organs including pituitary, plays a major role in proteolytic cleavage of peptide hormones (e.g., POMC) and neuropeptide precursors. PCSK1 null mice and humans with loss-of-function PCSK1 mutations exhibit multiple endocrine defects [34,35]. Thus, in the excess GH1-treated pituitary, down-regulation of PCSK1 might lead to multiple endocrine defects as a result of impaired hormone processing (Table 2).

Taken together, the balance and regulation of various hormones in the pituitary were influenced by excess GH1 treatment. The induced imbalance of pituitary hormones might affect the regulation of many biological and physiological functions in excess GH1-treated salmon.

3.1.2. *Cell growth and cell proliferation*

In our proteome analysis, we investigated differential expression dynamics of proteins, including metabolic enzymes, ribosomal proteins, and proliferation related proteins, in the excess GH1-treated pituitary. Aldolase C (ALDOC), triosephosphate isomerase 1 (TPI1), and glyceraldehyde-3-phosphate dehydrogenase (GAPDH) are enzymes of the glycolytic pathway, involved in the conversion of glucose into lactate or pyruvate. Mitochondrial

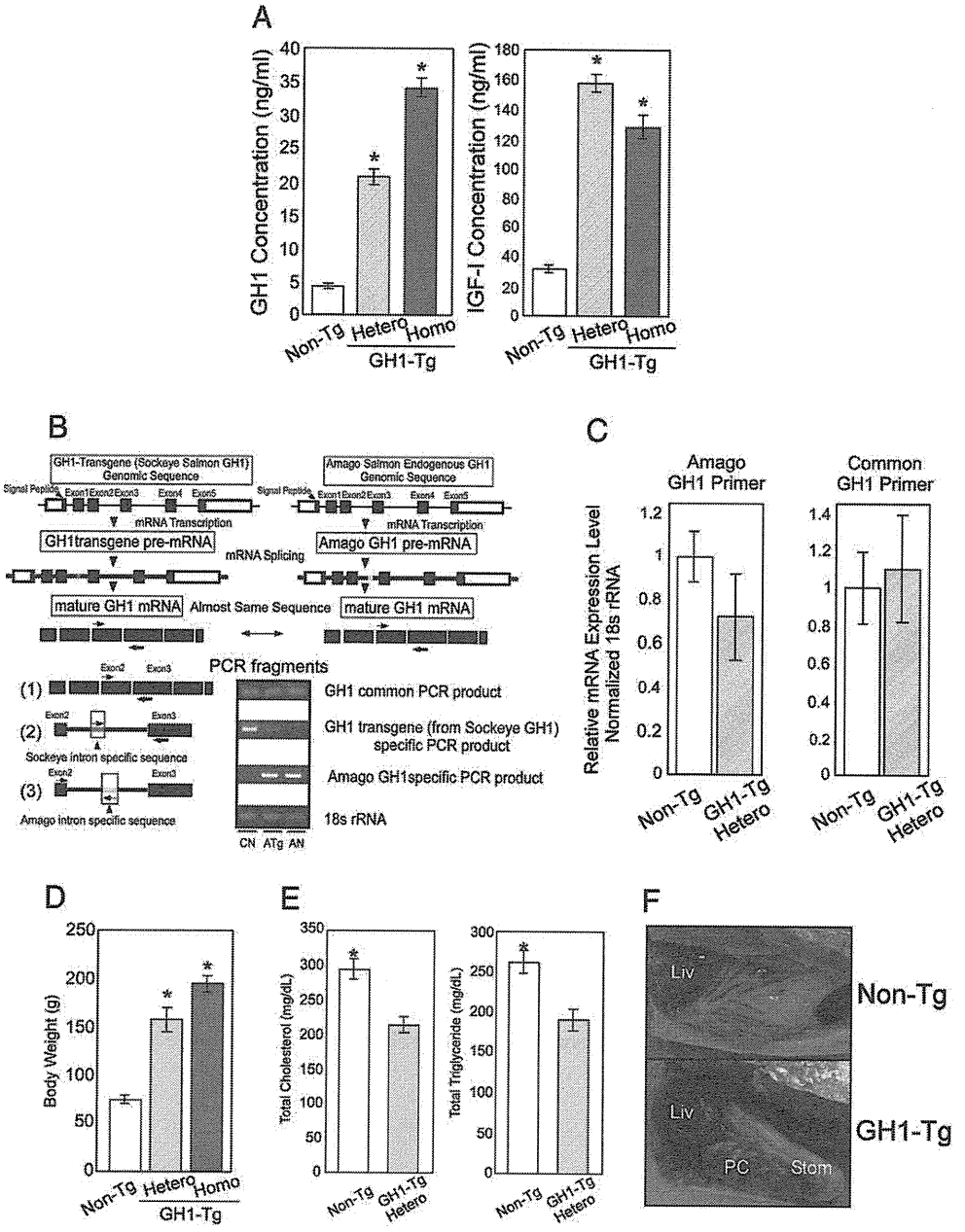

Fig. 3 – Characteristics of transgenic amago salmon overexpressing type 1 growth hormone (GH1). (A) The concentration of GH1 and IGF-I in plasma. GH1 and IGF-I levels in plasma were determined by ^{125}I-based radioimmuno assay. (B) Exon–intron structure of GH1-transgene (sockeye salmon) and amago salmon GH1 gene. To distinguish between amago salmon endogenous GH1 gene and sockeye salmon transgenic GH1 gene, primer sets used in reverse transcription (RT) PCR were designed against the region between exon 2 and exon 3, as follows: (1) GH1 common primers, which amplify both genes; (2) GH1 transgene-specific primers, which amplify only the sockeye salmon transgenic GH1 gene; and (3) amago-specific primers, which amplify only the endogenous amago salmon GH1 gene, respectively. CN, ATg, and AN indicated non-Tg coho salmon (*Oncorhynchus kisutch*), GH1-Tg amago salmon integrated sockeye salmon GH1 gene, and non-Tg amago salmon, respectively. Coho salmon DNA was also used for positive control to GH1 transgene-specific (the sockeye salmon transgenic GH1) primers and negative control to amago-specific primers. (C) GH1 mRNA levels in the pituitary, determined by qRT-PCR using primer sets (1) and (3) described in Fig. 3B. (D) Comparison of body weights among GH1-Tg (homo- and heterozygous) amago and non-Tg amago. (E) Total cholesterol and triglyceride concentrations in plasma derived from GH1-Tg heterozygotes and non-Tg amago. (F) Representative visceral fat of non-Tg (top) and GH1-Tg heterozygous (bottom) amago. "Liv", "PC", and "Stom" indicate liver, pyloric caeca, and stomach, respectively. Asterisks denoted significant differences between non-Tg and GH1-Tg amago at $p<0.05$ by one-way ANOVA (A, D) or Student's t-test (C, E).

ATP synthase subunit β (ATP5B) is a catalytic core subunit of mitochondrial membrane ATP synthase, and plays a crucial role of mitochondrial oxidative phosphorylation (OXPHOS). In comparison with proliferating cells, quiescent cells exhibit a decrease in expression of glycolytic enzymes and an increase in expression of OXPHOS related enzymes [36–38]. In this study, we observed down-regulation of ALDOC, TPI1, and GAPDH, and up-regulation of ATP5B in the excess GH1-treated pituitary (Table 2). Reduction of ribosomal protein also causes attenuation of cell proliferation [39,40]. In the excess GH1-treated pituitary, 60S ribosomal protein P2 (RPLP2) and L24 (RPL24) were decreased (Table 2). Furthermore, an increase in ubiquitin-specific peptidase 7 (USP7), which is a deubiquitinating enzyme and stabilizes various proteins like p53, MDM2 p53-binding protein, and RE1-silencing transcription factor, is predicted to induce a reduction in cell proliferation and differentiation [41–43]. Inhibition of apoptosis inducing factor 1 (AIFM1), a flavoprotein with an oxidoreductase enzymatic activity, would induce cell cycle arrest and the suppression of cell proliferation [44]. A decrease in cold-inducible RNA-binding protein (CIRBP), an RNA-binding protein involved in a variety of stress response and disease processes in various cell types, would induce a reduction in cell proliferation, viability, and stress response ability [45,46]. The expression level of prothymosin α (PTMA), a nuclear acidic protein, is correlated to proliferation activity in a pituitary cell line (GH1 cell) [47]. In the excess GH1-treated pituitary, up-regulation of USP7 and down-regulation of AIFM1, CIRBP, and PTMA were detected (Table 2). Thus, our results suggest that GH1 treatment might cause cell cycle arrest and the suppression of cell proliferation in the salmon pituitary.

3.1.3. *Lipid metabolism*

In the excess GH1-treated pituitary, the expression levels of malic enzyme 3 (ME3) and fatty acid synthase (FASN), which are lipid metabolism-related enzymes, were altered. ME3 catalyzes the conversion of malate to pyruvate, producing NADPH [48]. FASN plays a role in *de novo* biogenesis of long-chain fatty acids via utilization of NADPH [49]. Thus, up-regulation of ME3 and down-regulation of FASN in the excess GH1-treated pituitary suggest that excess GH1 treatment induces cells to suppress lipid synthesis (Table 2).

3.2. *Protein profile in the GH1 transgenic salmon*

3.2.1. *Characteristics of GH1 transgenic salmon*

To confirm that protein dynamics in the excess GH1-treated pituitary are the same as those *in vivo*, we generated a GH1-Tg amago salmon. The GH1 transgene, consisting of a sockeye salmon GH1 gene under the control of the metallothionein B (MT-B) promoter, was integrated into the amago salmon genome, resulting in over-expression of GH1 throughout the whole body. In the plasma of GH1-Tg amago salmon (both homo- and heterozygous), the concentrations of GH1 and GH1-induced IGF-I were markedly elevated (Fig. 3A). To investigate the expression level of GH1 in the pituitary of GH1-Tg amago salmon, we performed qRT-PCR analysis using three primer sets: (1) GH1 common primer, (2) GH1 transgene (from sockeye salmon) specific primer, and (3) endogenous GH1 (from amago salmon) specific primer (Fig. 3B), which can detect a total GH1, GH1 from the transgene, and endogenous GH1, respectively (Fig. 3B). qRT-PCR analysis using these primer sets indicated that, in the pituitary, GH1 transgenesis has an insignificant effect on total of GH1, because endogenous GH1 expression is down-regulated by *in vivo* GH1 regulation system that is activated by the increase in the level of transgenic GH1 (Fig. 3C). However, GH1 transgenesis had a variety of effects on the phenotypes of GH1-Tg amago salmon. Compared to non-Tg amago salmon, the average body weights of heterozygous and homozygous GH1-Tg individual were ~2- and 3-

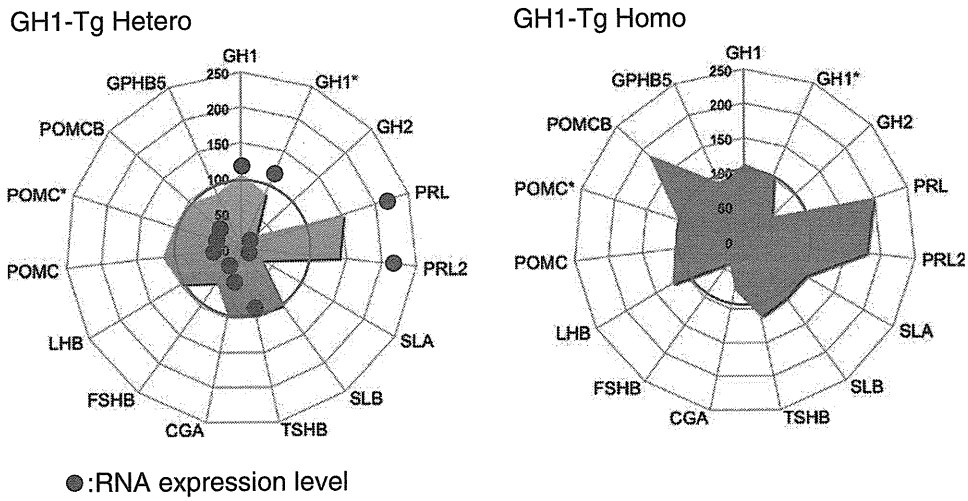

Fig. 4 – Comparison of expression levels of pituitary hormones in the GH1-Tg (homo- and heterozygous) and non-Tg pituitary by proteome and transcriptome analysis. Blue and red charts show that expression levels of pituitary hormones detected by proteome analysis in the pituitary of GH1-Tg (homo- and heterozygous). Asterisks indicate isoforms of identical pituitary hormones. Red circles indicate expression levels of pituitary hormones in non-Tg pituitary. Blue dots indicate expression levels of pituitary hormones obtained from subtractive microarray analysis. Each level represents the average among spots corresponding to each hormone gene. GH1/GH2 and PRL/PRL2 have highly similar sequences within each pair.

fold larger, respectively (Fig. 3D). In addition, GH1-Tg amago salmon exhibited enhancement of feeding behavior, shrinkage of the pituitary, and reduction of fertility, as do other GH1-Tg fish [5,17,50]. Furthermore, levels of total triglyceride and total cholesterol in the plasma of GH-Tg amago salmon were significantly decreased (Fig. 3E). Moreover, GH1-Tg amago salmon exhibited a reduction in visceral fat (Fig. 3F). These phenotypes were consistent with changes in protein expression levels observed in the excess GH1-treated pituitary.

3.2.2. *Identification of proteins and genes expressed in the GH1-Tg pituitary*

Proteins expressed specifically in the GH1-Tg pituitary were investigated by iTRAQ-MS/MS, resulting in the identification of 86 unique proteins that exhibit differential expression (≥1.25-fold change) in the GH1-Tg homozygous and/or heterozygous pituitary. Among them, 50 proteins did not change in the pituitary in response to excess GH1 treatment; 36 proteins were differentially regulated in excess GH1-treated pituitary. In the 36 proteins, the expression of the 28 proteins in the GH1-Tg homozygous and/or heterozygous pituitary showed similar pattern of the expression compared with excess GH1-treated pituitary, however, the expression of the remaining 8 proteins showed opposite expression pattern compared with that of excess GH1 treatment (Supplementary Table 1). The change in hormone balance in the GH1-Tg pituitary was almost identical to what was observed in the excess GH1-treated pituitary, except that SLA level did not change in the pituitary of the GH1-Tg homozygote (Figs. 2 and 4).

Additionally, we prepared customized amago salmon-specific subtractive microarrays using 1920 sequences (1915 amago cDNAs and 5 control DNAs). From the microarray analysis of mRNA levels in the pituitary, 45 genes (148 spots) listed in Supplementary Table 2 exhibited significant changes in the GH1-Tg amago heterozygote (fold change >1.5, $p<0.05$). The GH-Tg pituitary exhibited up-regulation of PRL/PRL2 and down-regulation of GH2, SLA, CGA and FSHB, just as in the excess GH1-treated pituitary; the mRNA levels of POMC and POMCB were markedly down-regulated (Fig. 4). These results were consistent with the down-regulation of GH gene expression in the pituitary from GH1-Tg salmon [50]. Bioinformatic analysis suggested that most of these differentially regulated molecules are involved in endocrine systems, metabolism, cell growth and proliferation (Supplementary Fig. 2).

4. Conclusion

In this study, excess GH1 treatment induced differential expression of pituitary proteins involved in endocrine systems, metabolism, cell proliferation and growth. In addition, the same protein dynamics were observed in the pituitary of GH1-Tg amago salmon. Furthermore, the characteristics predicted from these protein dynamics corresponded to the phenotypes of GH1-Tg salmon; these include enhancement of somatic growth and feeding behavior, shrinkage of the pituitary, reduction of fertility, and imbalances of lipid metabolism. Based on the results described above, we hypothesize that the regulation of hormone production and lipid metabolism are important to the enhancement of salmon somatic growth in response to GH1 treatment for the purpose of productivity improvement.

Supplementary materials related to this article can be found online at doi:10.1016/j.jprot.2011.12.009.

Acknowledgments

We are grateful to Dr. Hironori Ando for the technical advice about pituitary organ culture and to Dr. Koichiro Kano and Dr. Yoshinao Oki for IPA support. This work was supported in part by the Special Coordination Funds for Promoting Science and Technology "Creation of Innovation Centers for Advanced Interdisciplinary Research Areas" (to H.H.) and in part by the special subsidies for private school of Japan 14360104 (to T.M.) and Japanese grants 17380120 (to T.M. and H.H.) from the Ministry of Education, Culture, Sports, Science, and Technology, Japan.

REFERENCES

[1] Weltzien FA, Norberg B, Helvik JV, Andersen Ø, Swanson P, Andersson E. Identification and localization of eight distinct hormone-producing cell types in the pituitary of male Atlantic halibut (*Hippoglossus hippoglossus* L.). Comp Biochem Physiol A Mol Integr Physiol 2003;134:315–27.
[2] Ooi GT, Tawadros N, Escalona RM. Pituitary cell lines and their endocrine applications. Mol Cell Endocrinol 2004;228:1–21.
[3] Breves JP, Seale AP, Helms RE, Tipsmark CK, Hirano T, Grau EG. Dynamic gene expression of GH/PRL-family hormone receptors in gill and kidney during freshwater-acclimation of Mozambique tilapia. Comp Biochem Physiol A Mol Integr Physiol 2011;158:194–200.
[4] Ben-Jonathan N, Hugo ER, Brandebourg TD, LaPensee CR. Focus on prolactin as a metabolic hormone. Trends Endocrinol Metab 2006;17:110–6.
[5] Sundström LF, Devlin RH, Johnsson JI, Biagi CA. Vertical position reflects increased feeding motivation in growth hormone transgenic coho salmon (*Oncorhynchus kisutch*). Ethology 2003;109:701–12.
[6] Sambroni E, Abdennebi-Najar L, Remy JJ, Le Gac F. Delayed sexual maturation through gonadotropin receptor vaccination in the rainbow trout *Oncorhynchus mykiss*. Gen Comp Endocrinol 2009;164:107–16.
[7] Wong AO, Zhou H, Jiang Y, Ko WK. Feedback regulation of growth hormone synthesis and secretion in fish and the emerging concept of intrapituitary feedback loop. Comp Biochem Physiol A Mol Integr Physiol 2006;144:284–305.
[8] Agellon LB, Davies SL, Lin CM, Chen TT, Powers DA. Rainbow trout has two genes for growth hormone. Mol Reprod Dev 1988;1:11–7.
[9] Mori T, Deguchi F, Ueno K. Differential expression of Gh1 and Gh 2 genes by competitive RT-PCR in rainbow trout pituitary. Gen Comp Endocrinol 2001;123:137–43.
[10] Melmed S. Acromegaly pathogenesis and treatment. J Clin Invest 2009;119:3189–202.
[11] Perrini S, Laviola L, Carreira MC, Cignarelli A, Natalicchio A, Giorgino F. The GH/IGF1 axis and signaling pathways in the muscle and bone: mechanisms underlying age-related skeletal muscle wasting and osteoporosis. J Endocrinol 2010;205:201–10.
[12] Rius-Francino M, Acerete L, Jiménez-Amilburu V, Capilla E, Navarro I, Gutiérrez J. Differential effects on proliferation of GH and IGFs in sea bream(*Sparus aurata*) cultured myocytes. Gen Comp Endocrinol 2011;172:44–9.

[13] Madsen K, Friberg U, Roos P, Edén S, Isaksson O. Growth hormone stimulates the proliferation of cultured chondrocytes from rabbit ear and rat rib growth cartilage. Nature 1983;304:545–7.
[14] Johnsson Jorgen I, Bjornsson Bjorn Th. Growth hormone increases growth rate, appetite and dominance in juvenile rainbow trout, *Oncorhynchus mykiss*. Anim Behav 1994;48:177–86.
[15] Devlin RH, Sakhrani D, Tymchuk WE, Rise ML, Goh B. Domestication and growth hormone transgenesis cause similar changes in gene expression in coho salmon (*Oncorhynchus kisutch*). Proc Natl Acad Sci USA 2009;106: 3047–52.
[16] Devlin RH, Biagi CA, Yesaki TY. Growth, viability and genetic characteristics of GH transgenic coho salmon strains. Aquaculture 2004;236:607–32.
[17] Rahman MA, Mak R, Ayad H, Smith A, Maclean N. Expression of a novel piscine growth hormone gene results in growth enhancement in transgenic tilapia (*Oreochromis niloticus*). Transgenic Res 1998;7:357–69.
[18] Sheridan MA. Effects of thyroxin, cortisol, growth hormone, and prolactin on lipid metabolism of coho salmon, *Oncorhynchus kisutch*, during smoltification. Gen Comp Endocrinol 1986;64:220–38.
[19] Krasnov A, Agren JJ, Pitäknen TI, Mölsä H. Transfer of growth hormone (GH)transgenes into Arctic charr. (*Salvelinus alpinus* L.) II. Nutrient partitioning in rapidly growing fish. Genet Anal 1999;15:99–105.
[20] Falcón J, Besseau L, Fazzari D, Attia J, Gaildrat P, Beauchaud M, et al. Melatonin modulates secretion of growth hormone and prolactin by trout pituitary glands and cells in culture. Endocrinology 2003;144:4648–58.
[21] Shilov IV, Seymour SL, Patel AA, Loboda A, Tang WH, Keating SP, et al. The Paragon Algorithm, a next generation search engine that uses sequence temperature values and feature probabilities to identify peptides from tandem mass spectra. Mol Cell Proteomics 2007;6:1638–55.
[22] Tang WH, Shilov IV, Seymour SL. Nonlinear fitting method for determining local false discovery rates from decoy database searches. J Proteome Res 2008;7:3661–7.
[23] Mori T, Hiraka I, Kurata Y, Kawachi H, Mano N, Devlin RH, et al. Changes in hepatic gene expression related to innate immunity, growth and iron metabolism in GH-transgenic amago salmon (*Oncorhynchus masou*) by cDNA subtraction and microarray analysis, and serum lysozyme activity. Gen Comp Endocrinol 2007;151:42–54.
[24] Shimizu M, Swanson P, Fukada H, Hara A, Dickhoff WW. Comparison of extraction methods and assay validation for salmon insulin-like growth factor-I using commercially available components. Gen Comp Endocrinol 2000;119:26–36.
[25] Swanson P. Radioimmunoassay of fish growth hormone, prolactin, and somatolactin. In: Hochachka PW, Mommsen TP, editors. Analytical Techniques. Biochemistry and Molecular Biology of Fishes. Amsterdam: Elsevier Inc; 1994. p. 545–56.
[26] Moriyama S, Swanson P, Nishii M, Takahashi A, Kawauchi H, Dickhoff WW, et al. Development of a homologous radioimmunoassay for coho salmon insulin-like growth factor-I. Gen Comp Endocrinol 1994;96:149–61.
[27] Mori T, Kawachi H, Imai C, Sugiyama M, Kurata Y, Kishida O, et al. Identification of a novel uromodulin-like gene related to predator-induced bulgy morph in anuran tadpoles by functional microarray analysis. PLoS One 2009;4:e5936.
[28] Jiang Q, Ko WK, Lerner EA, Chan KM, Wong AO. Grass carp somatolactin: I. Evidence for PACAP induction of somatolactin-alpha and -beta gene expression via activation of pituitary PAC-I receptors. Am J Physiol Endocrinol Metab 2008;295:E463–76.
[29] Manzon LA. The role of prolactin in fish osmoregulation: a review. Gen Comp Endocrinol 2002;125:291–310.
[30] Chitalia VC, Foy RL, Bachschmid MM, Zeng L, Panchenko MV, Zhou MI, et al. Jade-1 inhibits Wnt signalling by ubiquitylating beta-catenin and mediates Wnt pathway inhibition by pVHL. Nat Cell Biol 2008;10:1208–16.
[31] Waite E, Lafont C, Carmignac D, Chauvet N, Coutry N, Christian H, et al. Different degrees of somatotroph ablation compromise pituitary growth hormone cell network structure and other pituitary endocrine cell types. Endocrinology 2010;151:234–43.
[32] Haisenleder DJ, Burger LL, Aylor KW, Dalkin AC, Marshall JC. Gonadotropin-releasing hormone stimulation of gonadotropin subunit transcription: evidence for the involvement of calcium/calmodulin-dependent kinase II (Ca/CAMKII) activation in rat pituitaries. Endocrinology 2003;144:2768–74.
[33] Wong AO, Li W, Leung CY, Huo L, Zhou H. Pituitary adenylate cyclase-activating polypeptide (PACAP) as a growth hormone (GH)-releasing factor in grass carp. I. Functional coupling of cyclic adenosine 3′,5′-monophosphate and Ca2+/calmodulin-dependent signaling pathways in PACAP-induced GH secretion and GH gene expression in grass carp pituitary cells. Endocrinology 2005;146:5407–24.
[34] Zhu X, Zhou A, Dey A, Norrbom C, Carroll R, Zhang C, et al. Disruption of PC1/3 expression in mice causes dwarfism and multiple neuroendocrine peptide processing defects. Proc Natl Acad Sci USA 2002;99:10293–8.
[35] Jackson RS, Creemers JW, Ohagi S, Raffin-Sanson ML, Sanders L, Montague CT, et al. Obesity and impaired prohormone processing associated with mutations in the human prohormone convertase 1 gene. Nat Genet 1997;16:303–6.
[36] López-Ríos F, Sánchez-Aragó M, García-García E, Ortega AD, Berrendero JR, Pozo-Rodríguez F, et al. Loss of the mitochondrial bioenergetic capacity underlies the glucose avidity of carcinomas. Cancer Res 2007;67:9013–7.
[37] Vander Heiden MG, Cantley LC, Thompson CB. Understanding the Warburg effect: the metabolic requirements of cell proliferation. Science 2009;324:1029–33.
[38] Cai Z, Zhao JS, Li JJ, Peng DN, Wang XY, Chen TL, et al. A combined proteomics and metabolomics profiling of gastric cardia cancer reveals characteristic dysregulations in glucose metabolism. Mol Cell Proteomics 2010;9: 2617–28.
[39] Chen A, Kaganovsky E, Rahimipour S, Ben-Aroya N, Okon E, Koch Y. Two forms of gonadotropin-releasing hormone (GnRH) are expressed in human breast tissue and overexpressed in breast cancer: a putative mechanism for the antiproliferative effect of GnRH by down-regulation of acidic ribosomal phosphoproteins P1 and P2. Cancer Res 2002;62:1036–44.
[40] Barna M, Pusic A, Zollo O, Costa M, Kondrashov N, Rego E, et al. Suppression of Myc oncogenic activity by ribosomal protein haploinsufficiency. Nature 2008;456: 971–5.
[41] Li M, Chen D, Shiloh A, Luo J, Nikolaev AY, Qin J, et al. Deubiquitination of p53 by HAUSP is an important pathway for p53 stabilization. Nature 2002;416:648–53.
[42] Li M, Brooks CL, Kon N, Gu W. A dynamic role of HAUSP in the p53-Mdm2 pathway. Mol Cell 2004;13:879–86.
[43] Huang Z, Wu Q, Guryanova OA, Cheng L, Shou W, Rich JN, et al. Deubiquitylase HAUSP stabilizes REST and promotes maintenance of neural progenitor cells. Nat Cell Biol 2011;13: 142–52.
[44] Schulthess FT, Katz S, Ardestani A, Kawahira H, Georgia S, Bosco D, et al. Deletion of the mitochondrial flavoprotein apoptosis inducing factor(AIF) induces

beta-cell apoptosis and impairs beta-cell mass. PLoS One 2009;4:e4394.
[45] Artero-Castro A, Callejas FB, Castellvi J, Kondoh H, Carnero A, Fernández-Marcos PJ, et al. Cold-inducible RNA-binding protein bypasses replicative senescence in primary cells through extracellular signal-regulated kinase 1 and 2 activation. Mol Cell Biol 2009;29:1855–68.
[46] Zeng Y, Kulkarni P, Inoue T, Getzenberg RH. Down-regulating cold shock protein genes impairs cancer cell survival and enhances chemosensitivity. J Cell Biochem 2009;107:179–88.
[47] Alvarez CV, Zalvide JB, Cancio E, Dieguez C, Regueiro BJ, Vega FV, et al. Regulation of prothymosin alpha mRNA levels in rat pituitary tumor cells. Neuroendocrinology 1993;57: 1048–56.
[48] DeBerardinis RJ, Lum JJ, Hatzivassiliou G, Thompson CB. The biology of cancer: metabolic reprogramming fuels cell growth and proliferation. Cell Metab 2008;7:11–20.
[49] Menendez JA, Lupu R. Fatty acid synthase and the lipogenic phenotype in cancer pathogenesis. Nat Rev Cancer 2007;7: 763–77.
[50] Mori T, Devlin RH. Transgene and host growth hormone gene expression in pituitary and nonpituitary tissues of normal and growth hormone transgenic salmon. Mol Cell Endocrinol 1999;149:129–39.

the FEBS Journal

Wild-type p53 enhances annexin IV gene expression in ovarian clear cell adenocarcinoma

Yusuke Masuishi[1,*], Noriaki Arakawa[1,*], Hiroshi Kawasaki[1], Etsuko Miyagi[2], Fumiki Hirahara[2] and Hisashi Hirano[1]

1 Department of Supramolecular Biology, Graduate School of Nanobioscience, Yokohama City University, Japan
2 Department of Obstetrics and Gynecology, Yokohama City University School of Medicine, Japan

Keywords
annexin IV; clear cell adenocarcinoma; ovarian cancer; p53; promoter

Correspondence
N. Arakawa or H. Hirano, Department of Supramolecular Biology Graduate School of Nanobioscience Yokohama City University, 1-7-29 Suehiro-cho, Tsurumi-ku, Yokohama 230-0045, Japan
Fax: +81 45 508 7667
Tel: +81 45 508 7247
E-mail: arakawa@yokohama-cu.ac.jp

*These authors contributed equally to this work

(Received 13 December 2010, revised 25 January 2011, accepted 21 February 2011)

doi:10.1111/j.1742-4658.2011.08059.x

The protein annexin IV (ANX4) is elevated specifically and characteristically in ovarian clear cell adenocarcinoma (CCA), a highly malignant histological subtype of epithelial ovarian cancer. On the basis of the hypothesis that the expression of *ANX4* in CCA is regulated by a unique transcription mechanism, we explored the *cis*-elements involved in CCA-specific ANX4 expression using a luciferase reporter. We compared the transcriptional activities of the region from −1534 to +1010 relative to the *ANX4* transcription start site in CCA and non-CCA-type cell lines, and found that two repeated binding motifs for the tumor suppressor protein, p53, in the first intron of *ANX4* were involved in CCA-specific transcriptional activity. Furthermore, chromatin immunoprecipitation showed that endogenous p53 bound to this site in CCA cell lines. Moreover, the use of short interference RNA to silence the *p53* gene decreased the transcriptional activity and mRNA expression of *ANX4* in CCA cell lines. Thus, the *ANX4* gene is, at least in part, regulated by p53 in CCA cells. Mutations in the *p53* gene were absent and levels of p53 target genes were higher in several CCA-derived cell lines. Although the expression of ANX4 is typically low in these non-CCA cell lines, ANX4 levels were elevated more than three-fold by the overexpression of wild-type but not mutant p53. Therefore, we conclude that the *ANX4* gene is a direct transcriptional target of p53, and its expression is enhanced by wild-type p53 in CCA cells.

Introduction

Epithelial ovarian carcinoma (EOC), which comprises the majority of ovarian cancers, is a leading cause of death among gynecological malignancies [1]. This disease is both morphologically and biologically heterogeneous, and can be divided into four major histological subtypes based on morphological criteria: serous, endometrioid, mucinous and clear cell carcinoma. Clear cell adenocarcinoma (CCA) is distinct histopathologically and clinically from the other EOC subtypes. Although the incidence of CCA is not high, patients with CCA have a markedly worse clinical prognosis than patients with other EOC subtypes. The recurrence of CCA is higher, even in the early stages, and the 3- and 5-year survival rates for CCA patients are significantly lower than for patients with other subtypes [2]. In addition, CCA shows a lower response to standard platinum-based chemotherapy. For these reasons, CCA is considered a highly malignant type of EOC.

CCA has several features that distinguish it from the other subtypes. The proliferative activity of CCA cells

Abbreviations
ANX4, annexin IV; CCA, clear cell adenocarcinoma; ChIP, chromatin immunoprecipitation; EOC, epithelial ovarian carcinoma; Mdm2, murine double minute 2; MMC, mitomycin C; NF-κB, nuclear factor-κB RNAi, RNA interference; siRNA, small interfering RNA.

is significantly lower than that of serous adenocarcinoma cells [3,4], which may help explain why CCA responds poorly to chemotherapy. Indeed, more patients are diagnosed during stage I of disease for CCA than for serous adenocarcinoma [5]. The tumor repressor gene *p53* is altered in 50–70% of advanced-stage EOC cells of all subtypes except CCA cells [6,7], in which it is only infrequently altered [8,9]. Furthermore, an immunohistochemical study of CCA tissue revealed a significant increase in the expression of the cyclin-dependent kinase inhibitor p21, a target of p53 [10]. Comprehensive gene expression profiling has revealed that the pattern of gene expression in CCA cells is clearly distinct from that of other EOC cells [11,12]. In particular, the annexin IV (annexin A4, ANX4) transcript is among a cluster of genes that are up-regulated in CCA cells. In addition, based on fluorescence 2D difference gel electrophoresis assays, it was previously shown [13] that ANX4 protein expression is markedly elevated in CCA-type cell lines and tissue compared to a mucinous adenocarcinoma-type cell line and tissue. Subsequently, Zhu *et al.* [14] compared proteomic patterns in 16 CCA and eight serous tissue samples, and also reported the up-regulation of ANX4 in all CCA tissues. More recently, in an immunohistological chemical study of more than 100 tissue samples of ovarian cancer patients, Kim *et al.* [15] found that more than 30 of the 43 CCA-type tissue samples were strongly positive for ANX4 compared to only five of the 62 serous-type samples. These findings suggest that the up-regulation of ANX4 is a unique characteristic of ovarian CCA.

ANX4 belongs to a ubiquitous family of calcium-dependent phospholipid-binding proteins. The function of the protein is assumed to differ between ANX isoforms [16]. Although little is known about the detailed physiological roles of ANX4, previous studies have reported the involvement of this protein in membrane permeability [17], exocytosis [18] and the regulation of ion channels [19]. Han *et al.* [20] and Kim *et al.* [15] reported that the level of ANX4 expression was associated with chemoresistance in human cancer cell lines. Therefore, it was suggested that ANX4 might constitute a novel therapeutic target for overcoming resistance to cancer chemotherapy in patients with ovarian CCA.

The elucidation of the molecular mechanisms regulating CCA-specific ANX4 expression may lead to a better understanding of the molecular biology unique to CCA cells, which is important for overcoming the malignancy of this disease. However, the mechanisms regulating the transcription of the *ANX4* gene have not been elucidated. In the present study, we characterized the flanking region of the transcription start site for *ANX4* and identified an intronic enhancer essential to the up-regulation of *ANX4* expression in CCA cells. We also found that the wild-type p53 protein binds to this region and acts as a positive regulator of *ANX4* gene expression in ovarian CCA.

Results

CCA-specific expression of ANX4

We previously found (using 2D difference gel electrophoresis analysis) that the amount of ANX4 was significantly higher in CCA than non-CCA cell lines and tissues [13]. We confirmed this finding by western blotting and real-time RT-PCR analyses using cell lines originating from CCA, OVTOKO and OVISE cultured cell lines, as well as the mucinous type of EOC, MCAS. ANX4 was detected strongly in OVTOKO and OVISE cells but not in MCAS cells (Fig. 1A). In the real-time RT-PCR experiment, the expression level of ANX4 mRNA was nine- and four-fold higher in OVTOKO and OVISE cells, respectively, than in

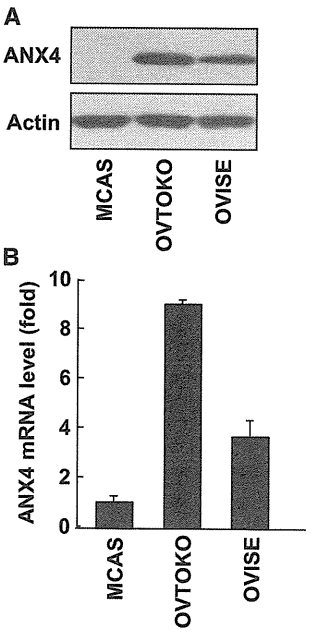

Fig. 1. ANX4 is up-regulated in CCA cell lines. Protein and RNA were extracted from two CCA (OVTOKO and OVISE) cells lines and one non-CCA (MCAS) cell line, and then ANX4 protein (A) and mRNA (B) levels were compared by western blotting and real-time RT-PCR analyses, respectively. Actin was included as a loading control. The values were normalized to the level of 18S ribosomal RNA expression in each sample. Bars represent the mean ± SE of three experiments.

MCAS cells (Fig. 1B). These results indicate that the expression level of ANX4 is increased in CCA cell lines compared to non-CCA cell lines, as demonstrated previously [13,15], and that ANX4 expression is controlled at the level of transcription. To determine the transcriptional factor responsible for these different expression levels of ANX4, we performed promoter/enhancer analysis of the *ANX4* gene using these three cell lines.

Determination of the 5′-end of the ANX4 mRNA

To determine the 5′-end of ANX4 mRNA, 5′-RACE analysis was performed using RNA isolated from MCAS, OVTOKO and OVISE cultured cell lines. Single DNA bands of the same size (170 bp) were detected for each cell line by agarose gel electrophoresis of the 5′-RACE products (Fig. 2A). Sequence analyses verified that each band had the same sequence, corresponding to the first through third exons of the ANX4 cDNA reported in the GenBank database (NM_001153.2), although the 5′-end identified in the present study was located upstream of the 5′-end reported in the database (Fig. 2B). We regarded the 5′-end determined by our 5′-RACE analysis as a putative transcription start site (+1) of *ANX4*.

The +180 region is essential for CCA-specific transcriptional activity of ANX4

To identify the *cis*-elements essential for CCA-specific expression of *ANX4*, we first isolated the region from −1534 to +1010 relative to the transcriptional start site and inserted it into a luciferase reporter vector (−1534/+1010 luc). Consensus TATA-box sequences were not found in the predicted positions of this region, although the region from −586 to +402 was identified as a CpG island (GC contents, 68%) using the software CPG ISLAND RESEARCHER (http://cpgislands.usc.edu/). The modified −1534/+1010 luc vector was

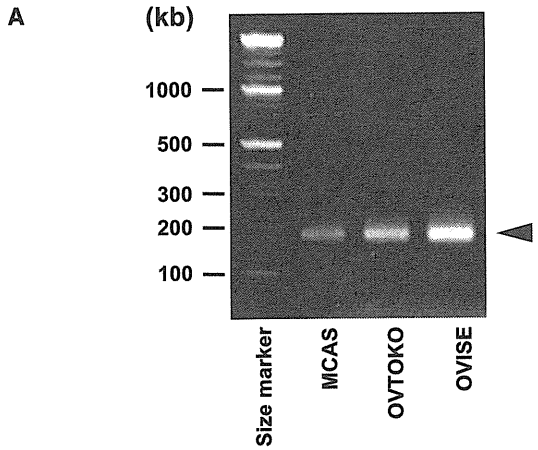

B

```
                                                    +1                                  *
-43  ggatccgtcccggataagacccgctgtctggccctgagtagggTGTGACCTCCGCAGCCGCAGAGGAGGAGCGCAGCCCGGCCTCGgtac  +47
+48  gaggggtaaaggggctccgggccgggggtcctgggctcagggaacggggagcgtggcccgggagcgtctcgcggggatgcccggctccgc  +137

                                                    ▼
+138 gctgcaccccagagtgggtgctcgccgccggcttgcgggcaagcccgggcggccacagggtggaggggccagcgggccctggactcgct  +227
                                      NF-kB
                                    NF-kB
                                     p53

                                                    ▽
+228 ccgggtgggcgagagggaggcgagcgcggtgcttaaccgctggcaccatccaggacatccagggccgcttacacggctcaggacgcgggt  +317
                                    v-Myb          GATA-1
```

Fig. 2. The 5′-end of the *ANX4* gene. To determine the transcriptional start site of *ANX4* in EOC cells, the 5′-end of ANX4 mRNA was investigated by 5′-RACE analysis. (A) Agarose gel electrophoresis of PCR products from the 5′-RACE procedure. The arrowhead indicates the bands detected in three cell lines by 5′-RACE. (B) The nucleotide sequence of the flanking region of the *ANX4* transcription start site and putative transcription factor-binding sites within this region. Uppercase letters indicate the first exon of *ANX4*. The asterisk and +1 show the 5′-ends reported in the GenBank database (NM_001153.2) and identified newly in the present study, respectively. The putative binding sequences for the representative transcription factors are underlined. The nucleotide positions at +180 and +270 are denoted by filled and unfilled triangles, respectively.

transfected into MCAS, OVTOKO and OVISE cells, and the transcriptional activity was determined by luciferase assay (Fig. 3A). The −1534/+1010 region demonstrated approximately nine- and four-fold higher levels of transcriptional activity in OVTOKO and OVISE cells, respectively, compared to MCAS cells. This result is very similar to the real-time RT-PCR data (Fig. 1B), suggesting that the −1534/+1010 region contains an element essential for CCA-specific expression of *ANX4*. Therefore, we constructed the various 5′- or 3′-deletion mutants of the modified −1534/+1010 luc vector, and measured the transcriptional activity of each mutant (Fig. 3A). Deletion of the 3′-downstream region (−42 to +1010) resulted in a marked decrease in luciferase activity in OVTOKO and OVISE cells, although no change occurred in MCAS cells. Further deletion of the 5′-upstream region from −181 decreased luciferase activity in all three cell lines. By contrast, the deletion of the 5′-upstream region from −43 alone also reduced luciferase activity in all three cell lines, although it did not completely diminish the higher activity seen in OVTOKO and OVISE cells. This CCA-preferential activity of the region between −43 and +1010 was removed by deleting the 3′-downstream region from +28. These results suggest that an element essential for CCA-specific expression of *ANX4* is present between +27 and +1010 in the downstream region of the transcription start site. To further focus on the region essential for CCA-specific gene expression, serial 3′-deletions were constructed and subjected to luciferase reporter analysis (Fig. 3B). Deletion from

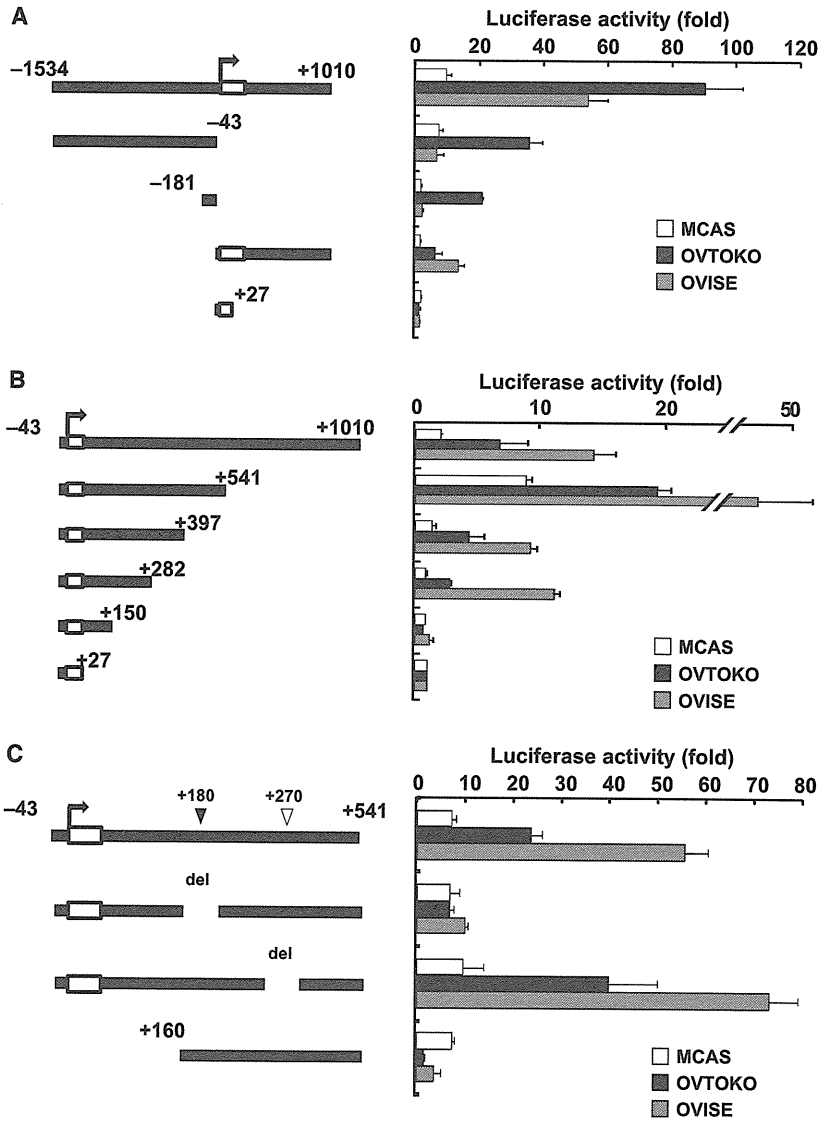

Fig. 3. CCA-specific transcriptional activity of *ANX4* depends on the +180 region in the first intron. The luciferase vector containing the flanking region of the *ANX4* transcriptional start site −1534/+1010 luc and its deletion mutants were introduced into OVTOKO, OVISE and MCAS cells, and the transcriptional activities were measured. Schematic diagrams of the *ANX4* promoter–luciferase plasmids are shown on the left, where the 5′- and 3′-ends are indicated relative to the transcription start site. (A) The 3′-downstream region of *ANX4* is essential for CCA-specific transcriptional activity. The luciferase activities of the full-length −1534/+1010 luc vector and the mutants with 5′-upstream or 3′-downstream deletions were compared. (B) The transcriptional activities of mutants with 3′-deletions in the region from −43 to +1010. (C) The effect of deleting the +180 or +270 regions on the transcriptional activities. Luciferase activity is expressed as the fold change relative to pGL3-basic vector activity in each cell. The β-galactosidase control vector was co-transfected as an internal control. Schematic diagrams of the *ANX4* promoter–luciferase plasmids are shown on the left, where the location of the 5′- and 3′-ends are indicated relative to the transcription start site. Bars represent the mean ± SE of at least three experiments.

+1010 up to +541, or from +541 to +397, resulted in marked changes in luciferase activity in all three cell lines. This suggests that the binding sites of both negative and positive regulatory transcription factors are contained in these two regions, although their role in ANX4 transcription is not specific to CCA cells. By contrast, the deletion of +282 to +150 decreased luciferase activity in OVTOKO and OVISE cells without altering activity in MCAS cells, suggesting that this region contains an element involved in CCA-specific expression of *ANX4*. In this region, the presence of putative transcription factor-binding sites was revealed by sequence analysis with the software TFSEARCH (http://www.cbrc.jp/research/db/TFSEARCH.html) and MOTIF (http://motif.genome.jp/) searching protein and nucleic acid sequence motifs. The nuclear factor (NF)-κB and p53-binding sites were found at position +180, and the GATA-binding site was found at position +270 (Fig. 2B). To determine which site was involved in CCA-specific *ANX4* expression, reporter analyses were performed using a luciferase construct containing the region −43 to +541 (−43/+541 luc) and mutants of this construct with regions at either +180 or +270 deleted. As shown in Fig. 3C, deleting the +270 region did not change the transcriptional activity of the −43/+541 luc of any cell line, whereas deleting the +180 region markedly decreased transcriptional activity in OVTOKO and OVISE cells but not in MCAS cells. Furthermore, CCA-specific transcriptional activity conferred by the +180 region was diminished by deleting the region upstream of +160. Accordingly, the +180 region acts as a transcription enhancer essential for the up-regulation of *ANX4* in CCA cells.

ANX4 expression is regulated by p53 in CCA

Potential binding sites for p53 and NF-κB were found in the +180 region (Fig. 2B). To determine whether these proteins conferred CCA-specific transcriptional activation of *ANX4*, two kinds of mutation patterns at the +180 region were designed. Both mutations, +180 mutA (5′-GGCCAAGCGTA-3′) and +180 mutB (5′-GGGAAAGCCCC-3′), abolished the putative p53-binding site. In addition, +180 mutA also destroyed the putative binding sequence for NF-κB, whereas +180 mutB maintained the NF-κB-binding sequence (5′-GGRNNYCC-3′). As shown in Fig. 4a, both +180 mutA and +180 mutB markedly decreased the transcriptional activity of the −43/+541 luc vector in OVTOKO and OVISE cells. Mutations at the +180 region reduced the transcriptional activity of the −1534/+1010 luc vector by half in CCA cells. Similar results were observed in the other EOC cell lines. Mutations at the +180 region significantly reduced transcriptional activity of the −43/+541 luc vector in the CCA cell lines RMG-I and RMG-II compared to the non-CCA cell lines OVCAR-3 and RMUG-S (Fig. S1). These results suggest that the +180 region acts as a p53-binding site in CCA cells.

The p53 protein binds to two copies of the motif 5′-RRRCWWGYYY-3′, separated by a variable spacer of length 0–13 bp [21]. The p53-binding motif in the +180 region matched this sequence exactly. Three sites at +161, +172 and +196 contained sequences similar to the p53-binding motif, although each was an incomplete motif. To determine whether these act as other

Fig. 4. p53 is a direct regulator of the *ANX4* gene in CCA. (A) The effect of mutating the +180 region on transcriptional activity. Two mutation patterns were made in the putative binding sequences for NF-κB and p53. In +180 mutA, both binding sequences were disrupted. In +180 mutB, the p53-binding sequence was disrupted, whereas the NF-κB-binding sequence had 100% consensus. These mutations were introduced into the indicated luciferase vectors. The β-galactosidase control vector was co-transfected with the luciferase vectors to normalize transfection efficiency. $*P < 0.05$ and $**P < 0.01$ versus −1534/+1010 luc. (B) The effect of mutating p53-binding motifs around the +180 region. The p53-binding motif-like sequences around the +180 region in the −43/+541 luc reporter were mutated (+180 mutA, +161 mut, +172 mut and +196 mut). The mutants were transfected into OVISE cells, and transcriptional activities were measured via luciferase assays. (C) p53 bound to the *ANX4* gene. ChIP assay was performed with OVISE, OVTOKO and MCAS cells and antibodies against p53. Immunoprecipitation of p53 protein–DNA complexes was conducted with control IgG or anti-p53 antibody (DO-1) or without antibody (noAb). Total lysate was used as a control for PCR amplification (input). PCR was performed with gene-specific primers for p21 and ANX4. As a positive control, p53 binding was tested with p21 specific primers targeting the genomic region harboring the p53-responsive element. The results displayed are representative of the findings from three independent experiments. (D) The expression levels of p53 in cells transfected with Stealth™ siRNA. Cell lines were transfected with siRNA and grown for 72 h, and then p53 protein levels were determined by western blotting. Representative western blots of three experiments are shown. Actin was included as a loading control. (E) The CCA-specific transcriptional activities of −43/+541 luc were suppressed by introducing p53 siRNA. siRNA-transfected cells were incubated for 24 h in one well of a 24-well plate, and then transfected with the −43/+541 luc vector and grown in culture for 24 h. The pRL-TK vector was co-transfected with the luc vector used as an internal control. (F) siRNA-transfected cells were grown for 72 h, and then the mRNA levels of ANX4 were quantified by real-time RT-PCR. All luciferase activity is expressed as the fold change relative to pGL3-basic vector activity. Schematic diagrams of the *ANX4* promoter–luciferase plasmids are shown on the left, where the location of the 5′- and 3′-ends are indicated relative to the transcription start site (A, B and E). All bars represent the mean ± SE of at least three experiments (A, B, E and F).

binding sites for p53, we introduced a mutation at each of these predicted sites in the −43/+541 luc vector, and compared the levels of transcriptional activity. As shown in Fig. 4B, similar to the mutation at +180, mutating the +196 region also significantly reduced transcriptional activity. Although incomplete on its own, the p53-binding motif in the +196 region was 6 bp distal to the motif in the +180 region. The two motifs separated by a 6 bp spacer length is consistent with the criteria for a p53-binding domain described by Vogelstein *et al.* [21]. These findings suggest that the motifs in the +180 and +196 regions might be targets for p53 binding.

To examine whether endogenous p53 actually binds to these regions in CCA cells, we performed chromatin immunoprecipitation (ChIP) assays using PCR analysis of the p53 binding domains regulating *ANX4* and *p21* after immunoprecipitation with the p53-specific anti-

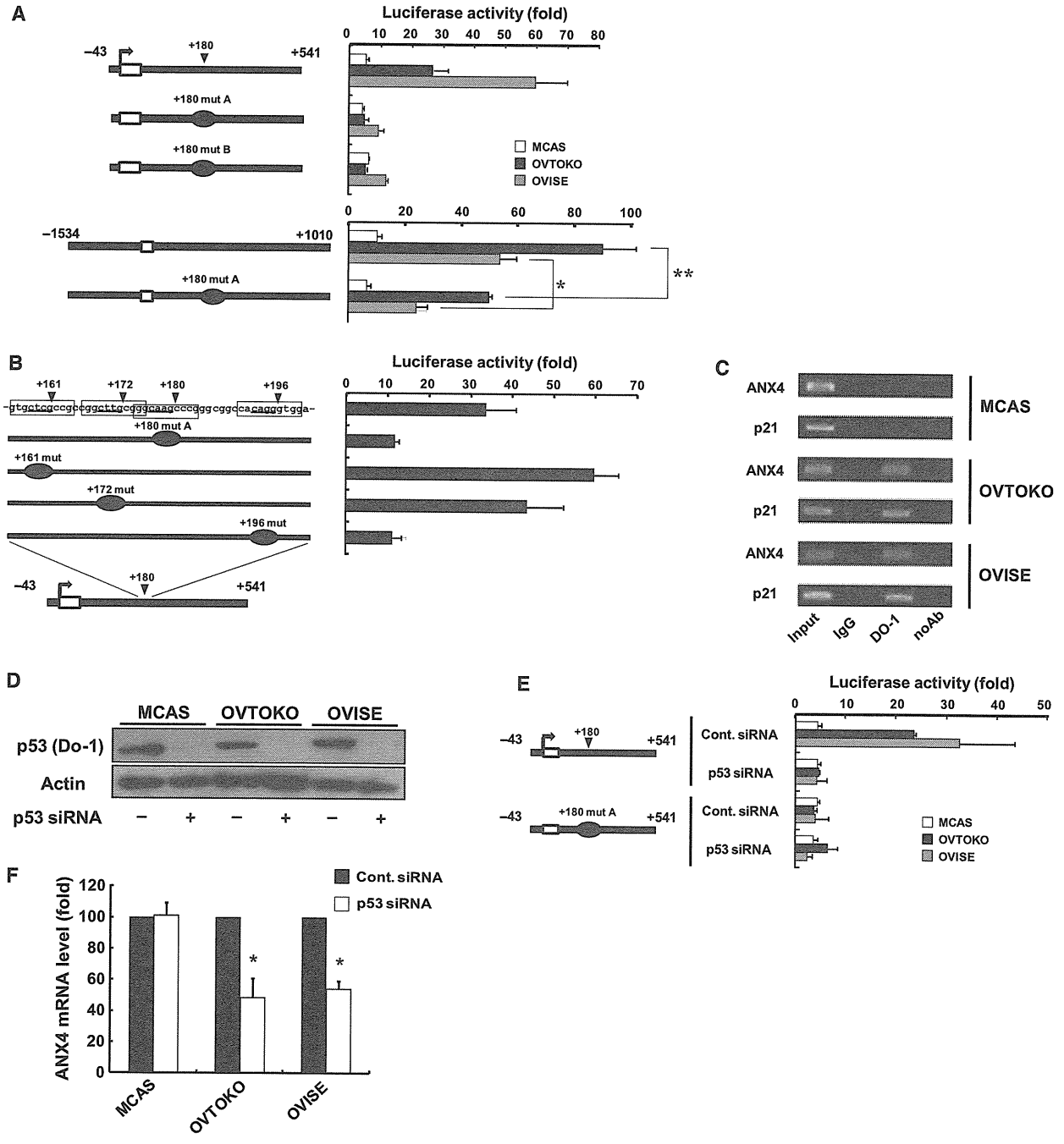

body DO-1 or normal IgG as a negative control. As shown in Fig. 4C, immunoprecipitation by the DO-1 antibody detected not only the *p21* promoter, but also the first intron of the *ANX4* gene in OVTOKO and OVISE cells but not in MCAS cells, indicating that endogenous p53 protein directly binds to the *ANX4* gene in CCA cells.

To verify the involvement of p53 in the CCA-specific expression of ANX4, we performed a gene-silencing experiment to suppress p53 protein expression. In cells transfected with a chemically modified small interfering RNA (siRNA) (Stealth™ siRNA) targeting p53 mRNA, the protein level of endogenous p53 markedly decreased (Fig. 4D). As shown in Fig. 4E, knockdown of p53 significantly reduced the transcriptional activity of the −43/+541 luc reporter in CCA cell lines but not in MCAS cells. By contrast, knockdown of p53 did not affect the activity of the reporter in any cell lines when the +180 region was mutated. These results indicate that p53 enhanced the transcriptional activity of *ANX4* via the +180 region. Similar data were obtained by knocking down p53 with another Stealth™ siRNA that targets a different site on the *p53* gene (data not shown). To confirm that the p53 protein actually regulates the expression of ANX4 mRNA, real-time RT-PCR analysis was conducted using the siRNA-transfected cells. As shown in Fig. 4F, introducing p53 siRNA reduced ANX4 mRNA in the CCA cell lines but did not affect ANX4 mRNA levels in the MCAS cells. These results indicate that *ANX4* is regulated by p53 in CCA cells.

Although the p53-directed siRNA completely diminished the CCA-specific transcriptional activity of the −43/+541 luc, it only reduced the ANX4 mRNA in CCA cells by approximately half. This discrepancy was also observed after mutations of the +180 region in the luciferase reporter vectors. In CCA cell lines, mutation of the +180 region completely diminished the transcriptional activity of −43/+541 luc, although the same mutation in −1534/+1010 luc, the reporter with the longest region, decreased transcriptional activity only by approximately half (Fig. 4A). Therefore, the transcriptional activation of *ANX4* in CCA is, at least in part, caused by p53, and other transcription factors with binding sites upstream of −43 or downstream of +541 might provide moderate additional transcriptional regulation.

ANX4 transcriptional activity correlates with the functional status of p53 in EOC cells

In almost all human cancers, p53 activity is lost as a result of mutation of the *p53* gene [22]. However, the above findings show that the *ANX4* gene is regulated by p53 in CCA cells, thereby suggesting that p53 is functional in CCA cells. To examine whether there is a correlation between the functional status of p53 and ANX4 transcriptional levels, we investigated *p53* gene mutations, as well as the expression levels of p53, ANX4 and typical p53 target genes. As shown in Fig. 5A, the p53 antibody DO-1 detected major bands near 53 kDa in EOC cell lines. Because the DO-1 antibody would also recognize p53β and p53γ, C-terminal truncated forms of the typical full-length p53 protein [23], the absence of bands at 46 kDa indicate that these proteins were not expressed in any of the EOC cell lines. Analysis of the *p53* cDNA sequences obtained from each cell line revealed no mutations in the CCA cell lines, whereas all non-CCA-type EOC cell lines had *p53* mutations (Table 1). Although the levels of p53 protein were lower in CCA cell lines, those of p53 target genes, p21 and murine double minute 2 (MDM2), as well as ANX4, were significantly higher in CCA cell lines than non-CCA-type EOC cell lines (Fig. 5A). In addition, in other cell lines carrying the wild-type *p53* gene, HEK293 or LNCaP cell lines, protein levels of ANX4, p21 and MDM2 were undetectable by western blotting (data not shown). Similar results were obtained by real time RT-PCR analyses; the mRNA levels of *p21* and *MDM2* were relatively lower in either HEK293, LNCaP or non-CCA-type EOC cell lines, which did not abundantly express ANX4 (Fig. 5B). These results suggest that there is a correlates between the functional status of p53 and ANX4 expression.

Wild-type p53 enhances the expression of the ANX4 gene

The results reported above suggest that the activation of wild-type p53 is one factor leading to ANX4 up-regulation in CCA. To examine whether wild-type p53 is actually involved in the transcriptional activation of *ANX4*, we transfected the −43/+541 luc and an expression plasmid containing wild-type p53 cDNA into MCAS, HEK293 and LNCaP cells (in which ANX4 levels are very low) and then conducted a luciferase assay. As shown in Fig. 6A, the overexpression of wild-type p53 resulted in a marked increase in *ANX4* transcriptional activity in each cell line. By contrast, transfection with the p53 mutants found in the non-CCA-type EOC cell lines, MCAS or OVCAR-3, did not alter luciferase activities in MCAS, HEK293 or LNCaP cells. As shown in Fig. 6B, ANX4 mRNA levels were substantially increased with the induction

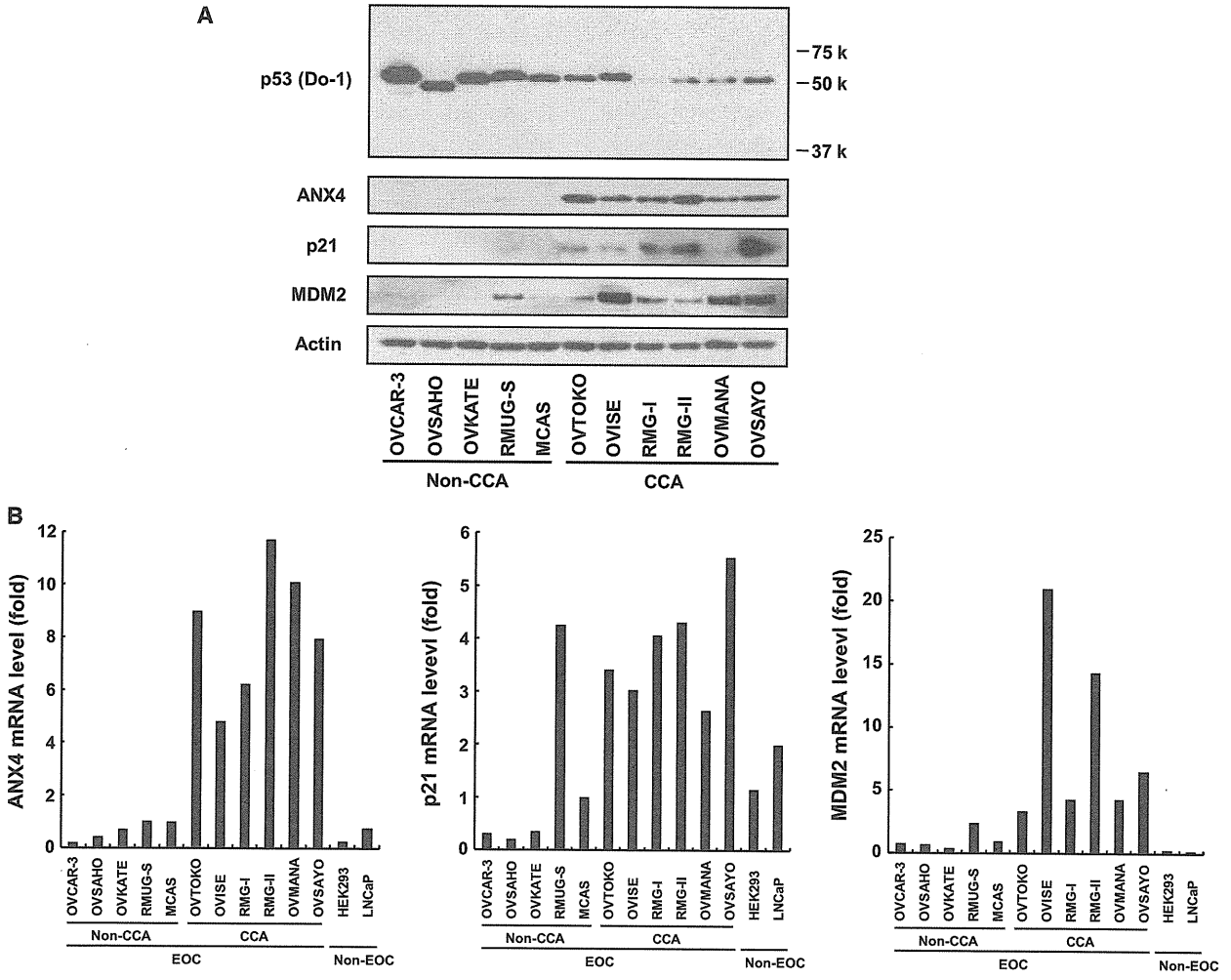

Fig. 5. ANX4 expression level correlates with p53 functional status. Protein and total RNA were extracted from various EOC cell lines, HEK293 and LNCaP cell lines. (A, B) Expression levels of protein and mRNA, and levels of p53, ANX4 and the known p53 targets, p21 and MDM2, were analyzed by western blotting (A) and real-time RT-PCR analyses (B), respectively. Actin protein levels were included in the western blotting analysis as a loading control. The relative mRNA levels were normalized to the level of 18S ribosomal RNA expression in each sample.

Table 1. p53 mutation lines used in the present study.

Cell line	Exon	Codon	Mutation	Amino acid change	EOC subtype
OVCAR-3	7	248	cgg → cag	R → Q	Serous
OVSAHO	10	342	cga → tga	R → Stop	Serous
OVKATE	8	282	cgg → tgg	R → W	Serous
RMUG-S	4, 10	72, 347	cgc → ccc, gcc → gtc	R → P, A → V	Mucinous
MCAS	4	114–125	Alternative sequence	LHSGTAKSVTCT → FTLWLP	Mucinous
OVTOKO	–	–	Not detected	–	Clear cell
OVISE	–	–	Not detected	–	Clear cell
RMG-I	–	–	Not detected	–	Clear cell
RMG-II	–	–	Not detected	–	Clear cell
OVMANA	–	–	Not detected	–	Clear cell
OVSAYO	–	–	Not detected	–	Clear cell
HEK293	–	–	Not detected	–	–
LNCaP	–	–	Not detected	–	–